11th International Science, Technology, Arts, Education, Management & the Social Sciences Conference
Lagos, Nigeria, June, 2018
Book of Proceedings Vol. 13 Series 1

Hydromagnetic Flow and Heat Transfer of a Micropolar Fluid over an Exponentially Stretching Vertical Sheet through a Porous Medium with Slip Effects

E. O. Fatunmbi[1] and A. Adeniyan[2]
[1]Department of Mathematics and Statistics, Federal Polytechnic, Ilaro, Nigeria
[2]Department of Mathematics, University of Lagos, Akoka, Lagos, Nigeria.
E-mail: [1]olusojiephesus@yahoo.com, [2]aadeniyan@unilag.edu.ng
Corresponding author: olusojiephesus@yahoo.com

ABSTRACT

This study examines steady, laminar, two-dimensional flow and heat transfer behaviour of dissipating and thermal radiating hydromagnetic Micropolar fluid over an exponentially stretching vertical sheet in a Darcy porous medium. The effects of velocity and thermal slips as well as viscous dissipation and Joule heating are also considered. The system of nonlinear partial differential equations governing the fluid flow is transformed into coupled system of nonlinear ordinary differential equations by appropriate similarity variables. The resulting system of boundary value differential equations is integrated via shooting method alongside fourth order Runge-Kutta integration scheme. Comparison with the previous results in some limiting situations shows a very good agreement. The effects of the controlling parameters on the dimensionless velocity, temperature and microrotation profiles are graphically presented and discussed. Also, the impacts of some selected flow parameters on the skin friction coefficient and heat transfer rates are tabulated for both Newtonian and non-Newtonian micropolar fluids. The results demonstrate that the values of the skin friction coefficient for a Newtonian fluid are higher than the corresponding values of the non-Newtonian micropolar fluid while the opposite response is the case for the rate of heat transfer.

Keywords: Hydromagnetic; Micropolar fluid; Exponentially stretching sheet; Slip effects.

1. INTRODUCTION

The theory of micropolar fluids developed and extended to thermo-micropolar fluid by Eringen [1966, 1972] has been an active area of research for scientists and engineers due to its significant applications in technological and industrial processes. This theory offers a good mathematical model for investigating the flow of complex and complicated fluids such as suspension solution, fluids with certain additives, animal blood, liquid crystals, polymeric fluids and clouds with dust (Chen et al., *2011*; Hayat *et al.,* 2011). Some areas of applications include polymer engineering, drug suspension in pharmacology, sediments in rivers, biological fluid modelling, crude oil extraction, food processing manufacturing and many others. These fluids are also found applicable in diverse areas of physics and engineering such as synovial lubrication, arterial blood flows, knee cap mechanics, cervical lows, pharmacodynamics etc. Micropolar fluids belong to non-Newtonian fluids with non-symmetric stress tensor which is capable of exhibiting certain microscopic effects arising from the local structure and micromotions of its elements. Such fluids posses complex nature and individual fluid particles may be of different shapes and may shrink and/or expand, occasionally changing shapes and rotating independently of the rotational movement of the fluid (Lukaszewicz, 1999).

In addition to the velocity vector in the classical Newtonian fluids, microplar fluids are characterised by two supplementary quantities: the spin, which accounts for the micromotions and the micro-inertia describing the distributions of atoms and molecules inside the fluid elements. Physically, micropolar fluids may represent fluids consisting of rigid, randomly oriented (or spherical) particles suspended in a viscous medium, where particles deformation is ignored. Peddieson and McNitt (1970) numerically obtained boundary layer equations for a microplar fluid which were applied to the problem of steady stagnation point flow and flow over a semi-infinite horizontal sheet. Thereafeter, several authors have investigated the boundary layer flow of micropolar fluids on different geometries and conditions (Ahmadi, 1976).

The boundary layer flow due to a stretching sheet has been found to have significant applications in engineering and industrial processes, for instance, drawing of plastic sheet, glass blowing, hot rolling, the cooling of metallic plate in a bath, annealing and thining of copper wires, textile and paper productions etc. Specifically, in many metallurgical operations such as the cooling of continuous strips or filaments drawn through a quiescent fluid, the strips are often stretched. In such cases, the quality of the end product depends to a great extent on the kinematics of stretching and the rate of cooling. When such strips are drawn in an electrically conducting fluid subjected to a magnetic field, the rate of cooling can be controlled and consequently a final product of desired characteristics can be obtained. Pioneering the work on boundary layer flow caused by stretching sheet, Crane (1970) investigated linearly stretching sheet on the steady two-dimensional problem and gave the similarity solution in closed analytical form. Gupta and Gupta (1977) extended the work of Crane to include heat and mass transfer on stretching sheet with suction or blowing. Eldabe *et al.*(2003) studied MHD flow of a micropolar fluid past a stretching sheet with heat transfer. Reddy (2012 examined heat generation and thermal radiation effects over a stretching sheet in a micropolar fluid.

The stretching of plastic sheet may not necessarily be linear in some practical situations, it may be nonlinear and/or the exponential type. In some cases, the rate of heat transfer at the stretching continuous surface occurs with exponential variations of stretching velocity and temperature distribution (Mukhopadhyay, 2013). Flow and heat transfer induced by an exponentially stretching sheet have numerous applications in technology such as in the case of annealing and thinning of copper wire. However, less attention has been given to the study of flow over an exponentially stretching sheet in spite of its important applications in many engineering operations. Magayari and Keller (1999) first studied the boundary layer flow, heat and mass transfer induced by an exponentially stretching sheet with exponential temperature distribution. El-Aziz (2009 extended the work of Magayari and Keller (1999) by investigating viscous dissipation effect on mixed convection flow of a micropolar fluid over an exponentially stretching sheet.

Mandal and Mukhopadhyay (2013) investigated heat transfer analysis for fluid flow over an exponentially stretching porous sheet with surface heat flux. Lately, Seini and Makinde (2013) studied MHD boundary layer flow of a Newtonian fluid due to exponential stretching surface with radiation and chemical reaction. Recently, Srinivasacharya and RamReddy (2011) examined the influence of Soret and Dufour effects on mixed convection from an exponenetially stretching surface using similarity solution deficient of removing the axial variable explicitly. Later, Adeniyan and Adigun (2016) offered a pure similarity solution of hydromagnetic boundary layer flow and heat transfer characteristics due to an exponentially stretching permeable vertical sheet with viscous dissipation and Joulean heating effects.

The applications of magnetic field in engineering problems are great. These include plasma studies, nuclear reactors, oil exploration, geothermal energy extractions, MHD generators, and boundary layer control in the field of aerodynamic. Similarly, fluid flow through porous medium is found useful in many areas of reservior engineering, such as crude oil extraction, ground water hydrology, In view of this, a number of reseachers have investigated MHD boundary layer flow in a porous medium. Olajuwon *et al.* (2014) examined heat and mass transfer in a hydromagnetic flow of a micropolar fluid over a porous medium. Recently, Fatunmbi and Fenuga (2017) studied MHD micropolar fluid flow over a permeable stretching sheet in the presence of variable viscosity and thermal conductivity with Soret and Dufour effects in a Darcy-Forchheimer porous medium.

Many of the engineering and manufacturing operations occur at high temperature hence, the effect of radiation transfer on magnetohydrodynamic flow, heat and mass becomes practically important for instance, in the design of relevant equipments as in, steel rolling, nuclear power plants, electric power generation, hypersonic flights, space vehicles, gas turbines. Due to these applications, many researchers have reported the influence of thermal radiation on fluid flow. Fatumnbi and Adeniyan (2018) examined MHD stagnation point-flow of micropolar fluids over a permeable stretching plate in porous media with thermal radiation, chemical reaction and viscous dissipation.

In all of the investigations metioned above, the authors assumed that the flow field obeys the no-slip boundary conditions which are the central tenets of the Navier-Stokes theory. On the contrary, it has been observed that the assumption of no-slip boundary conditions does not hold in some practical situations and it may be necessary to replace these with the partial slip boundary conditions. The slip and temperature jump boundary conditions represent a discontinuity in the transport variable across the interface and describe more accurately the non-equilibrium region near the surface. The assumption of partial slip on the flow field becomes important when considering particulate fluids e.g. emulsions, suspensions, foams and polymer solutions in which there may be a slip between the fluid and the boundary (wang, 2002). The applications of such study in technology can be found in the polishing of artificial heart valves and internal cavities (Mukhopadhyay, 2013) and in biomedical engineering e.g. blood flow through an artery (Bugliarello and Hayden, 1962; Nubar, 1971). To this end, Anderson, (2002) gave a closed form solution for the slip flow problem of a Newtonian fluid over a linearly stretching sheet, Das (2012) numerically studied slip effects on heat and mass transfer in hydromagnetic micropolar fluid flow over an inclined plate with variable fluid properties, thermal radiation and chemical reaction. It was found that the velocity distribution increases with the increase in the slip and thermal radiation parameters. Devi *et al.* (2015) examined radiation effect on MHD slip flow past a stretching sheet with variable viscosity and heat source/sink. Nandeppanavar *et al.* (2012) examined flow and heat transfer in MHD Newtonian fluid flow over a stretching sheet with variable thermal conductivity and partial slip.

Motivated by the above studies and keeping in mind the enormous applications of this type of study in various areas as highligted above, this work is undertaken to extend the work of Adeniyan and Adigun (2016). This extension is by considering the flow and heat transfer in an electrically conducting non-Newtonian microplar fluid induced by an exponentially stretching vertical sheet in a Darcy porous medium with velocity and thermal slips effects in addition to other physical parameters considered by the authors. With the use of appropriate similarity variables, the system of nonlinear partial differential equations governing the fluid flow is transformed into system of nonlinear ordinary differential equations and then solved via the shooting method alongside fourth order Runge-Kutta integration scheme.

1.1 Problem Formulation

Consider a steady, two-dimensional, dissipating and electrically conducting micropolar fluid flow over an exponentially stretching vertical sheet in a Darcy porous medium. The cartesian coordinate system is (x, y, z) while the corresponding velocity components are $(u, v\ 0)$. The x axis is directed towards the continuous stretching sheet along the flow while the y-axis is normal to it. The angular velocity is given as $\omega = (\omega_1, \omega_2, \omega_3) = (0, 0, N(x, y))$. The stretching velocity is assumed to be u_w while the sheet temperature is T_w and fluid suction/injection is imposed at the sheet surface. The flow is confined to the region $y \geq 0$. A transverse magnetic field $B = (0, B_0, 0)$ of strength B_0 is applied normal to the flow direction as shown in Fig. 1. The magnetic Reynolds number is assumed to be sufficiently small such that the induced magnetic field is negligible as compared to the applied magnetic field. The radiative heat flux term in x direction is considered negligible as compared to that in the y direction.

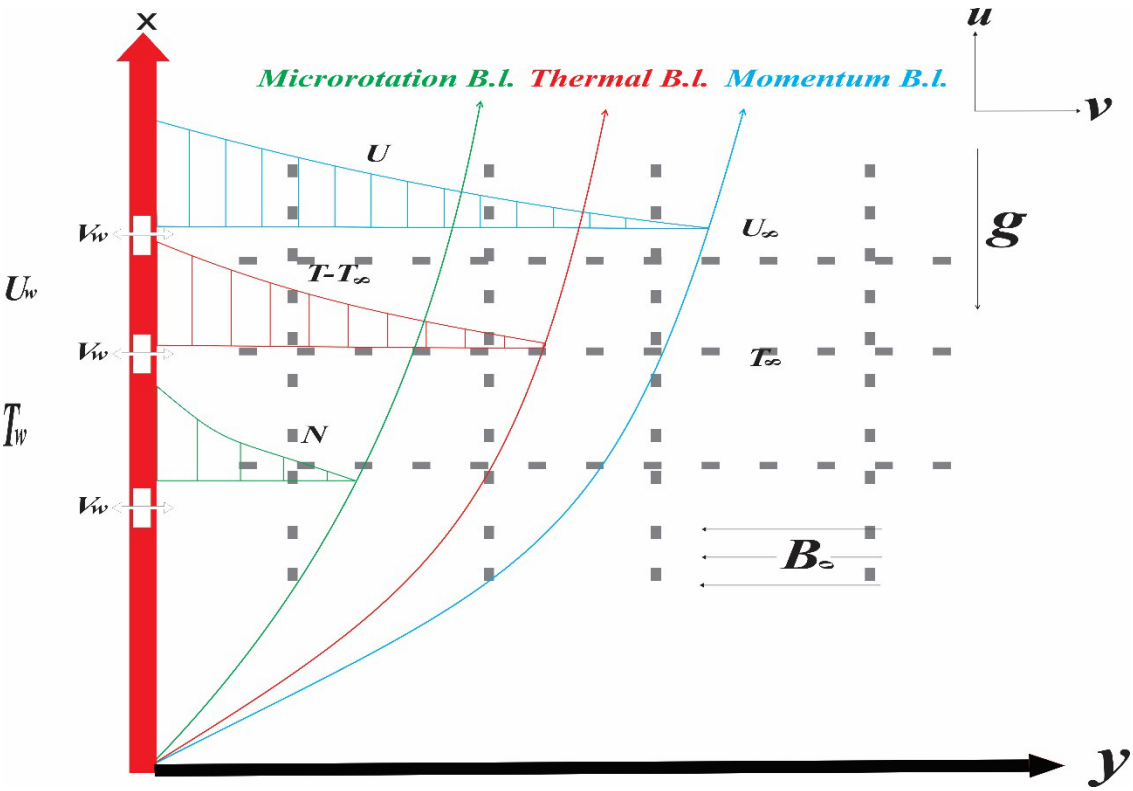

Fig. 1: Physical model and coordinate system

Under the stated assumptions, the Boussinesq approximation and the boundary layer approximations, the governing boundary layer continuity, momentum, microrotation and energy equations are respectively given as:

$$\frac{\partial u}{\partial x} + \frac{\partial v}{\partial y} = 0 \tag{1}$$

$$u\frac{\partial u}{\partial x}+v\frac{\partial u}{\partial y}=\frac{(\mu+\kappa)}{\rho}\frac{\partial^2 u}{\partial y^2}+\frac{\kappa}{\rho}\frac{\partial N}{\partial y}+g\beta_0(T-T_\infty)-\frac{\sigma B_0^2}{\rho}u-\frac{\mu}{\rho K_p}u \quad (2)$$

$$\rho j\left(u\frac{\partial N}{\partial x}+v\frac{\partial N}{\partial y}\right)=\gamma\frac{\partial^2 N}{\partial y^2}-\kappa\left(2N+\frac{\partial u}{\partial y}\right) \quad (3)$$

$$u\frac{\partial T}{\partial x}+v\frac{\partial T}{\partial y}=\frac{k}{\rho Cp}\frac{\partial^2 T}{\partial y^2}-\frac{1}{\rho Cp}\frac{\partial q_r}{\partial y}+\frac{(\mu+\kappa)}{\rho Cp}\left(\frac{\partial u}{\partial y}\right)^2+\frac{\mu}{\rho C_p K_p}u^2+\frac{\sigma B_0^2}{\rho Cp}u^2+\frac{q}{\rho C_p}(T-T_\infty). \quad (4)$$

The appropriate boundary conditions for Eqs. (1-4) are given by

$$y=0:\ u=U_w+A\frac{\partial u}{\partial y},\ v=V_w,\ N=-n\frac{\partial u}{\partial y},\ T=Tw+B\frac{\partial T}{\partial y} \quad (5)$$
$$y\to\infty:\ u\longrightarrow 0,\ N\longrightarrow 0,\ T\longrightarrow 0.$$

Where
u and v are the components of the velocity in x and y directions respectively,
ν is the coefficient of kinematic viscosity,
T is the fluid temperature,
β_0 is the thermal expansion coefficient.

Similarly, $u_w=U_0\,e^{\left(\frac{x}{L}\right)}$, $T_w=T_\infty+T_0e^{\left(\frac{2x}{L}\right)}$, U_0, T_0 and L are the stretching velocity, sheet temperature, a constant having the unit of speed for the stretching sheet, reference constant temperature and reference length respectively, T_∞ is the free stream temperature.

Following Makinde (2010), $\sigma=\sigma_0e^{\left(\frac{x}{L}\right)}$ is the electrical conductivity, $K_p=K_0e^{\left(\frac{x}{L}\right)}$ is the permeability of the porous medium, $V_w=V_0e^{\left(\frac{x}{2L}\right)}$, *is the* suction/injection ($V_w<0$ is suction, ($V_w>0$ is injection), g is the acceleration due to gravity, ρ is the density, C_p the specific heat at constant pressure, k is the thermal conductivity, B_0 is the constant magnetic strength and q_r is the radiative heat flux , N is the component of microrotation normal to $xy-$plane, $A=\alpha_1e^{-\left(\frac{x}{2L}\right)}$ is the velocity slip factor which changes with x, $B=\beta_1e^{-\left(\frac{x}{2L}\right)}$ is the thermal slip factor which changes with x (Mukhopadhyay [12]), μ is the dynamic viscosity, κ is the vortex or microrotation viscosity, C_p is the specific heat at constant pressure, $q=Q_0e^{\left(\frac{x}{L}\right)}$ is the heat source/sink, $j=j_0e^{-(x/L)}$ is micro-inertia density and $j_0=\frac{\nu L}{U_0}$, γ is the spin gradient viscosity while σ_0, Q_0, K_0 and V_0 are constants.

In the energy Eq. (4), the 5th and 6th terms indicate the viscous dissipation effect. The 5th term represents the viscous dissipation effect for a clear fluid while the 6th term is the viscous dissipation in the Darcy limit. Also, n is the microrotation surface boundary parameter with $0 \leq n \leq 1$. The case when $n = 0$ corresponds to $N = 0$ which indicates the vanishing of the spin on the boundary, also represents a strong concentration of the micro-particles such that the micro-particles close to the wall are unable to rotate as shown by Jena and Mathur [30].

The case $n = \frac{1}{2}$ indicates weak concentration of micro-particles and the vanishing of anti-symmetric part of the stress tensor (Ahmadi, 1976). The situation when $n = 1$ represents the vanishing of a linear combination of spin, shearing stress and couple stress which is an indication of turbulent boundary layer flows as reported by Peddieson [31].

It is to be noted also that when $\kappa = 0$, the velocity and microrotaion are decoupled and the macroscopic motion is unaffected by the microrotations. Similarly, when $\gamma = \kappa = j = 0$, the set of Eqs. (1-4) reduces to two-dimensional flow of incompressible Newtonian fluids.

Adeniyan (2015) as well as Akinbobola and Okoya (2015) and the references contained there-in have shown that the radiative heat flux q_r can have the structure

$$q_r = -\frac{4\sigma^*}{3\alpha^*}\frac{\partial T^4}{\partial y} \tag{6}$$

where σ^* is Stefan-Boltzmann constant and α^* is the mean absorption coefficient. With the assumption that that the fluid is in the optically thin limit and consequently doesn't absorb its own radiation but that emitted by the boundaries. Following the work of Adeniyan (2015) as well as Akinbobola and Okoya (2015) and the references contained ther-in we assume that the temperature differences within the flow are sufficiently small so that the T^4 can be expressed as a linear function, after expressing its Taylor series about the free stream temperature T_∞ and neglecting higher-order terms. This gives implies that:

$$T^4 \approx 4T_\infty^3 T - 3T_\infty^4 \tag{7}$$

Hence by using (7) in (6) we have

$$\frac{\partial q_r}{\partial y} = -\frac{16\sigma^* T_\infty^3}{3\alpha^*}\frac{\partial T^2}{\partial y} \tag{8}$$

The continuity Eq. (1) is satisfied by the introduction of the stream function defined by

$$u = \frac{\partial \psi}{\partial y}, \quad v - \frac{\partial \psi}{\partial x} \tag{9}$$

Also, Eqs. (2-5) are transformed into the corresponding ordinary differential equations by the following transformations (Seini and Makinde, 2013; Adeniyan and Adigun, 2016),

$$\psi = (2\nu L U_0)^{\frac{1}{2}} e^{\left(\frac{x}{2L}\right)} f(\eta), \quad \eta = y\left(\frac{U_0}{2\nu L}\right)^{\frac{1}{2}} e^{\left(\frac{x}{2L}\right)},$$
$$N = \left(\frac{U_0^3}{2\nu L}\right)^{\frac{1}{2}} e^{\left(\frac{3x}{2L}\right)}, \; T = T_\infty + T_0 e^{\left(\frac{2x}{L}\right)}\theta(\eta) \tag{10}$$

Thus, after substituting Eq. (10) into Eqs. (2--5) and using (8) gives nonlinear ODEs as:

$$(1+K)f''' + ff'' - 2f'^2 + Kg' + Gr\theta - H_D f' = 0 \tag{11}$$

$$\lambda g'' + fg' - 3f'g - 2KH(2g + f'') = 0 \tag{12}$$

$$\left(1+\frac{4}{3}R\right)\theta'' + \Pr(f\theta' - 4\theta f' + Q\theta) + PrEc\, f''^2 + PrEcH_D f'^2 = 0. \tag{13}$$

The boundary conditions become

$$\eta = 0: \; f' = 1 + \alpha f'', \; f = fw, \; g = -nf'', \theta = 1 + \beta\theta,$$
$$\eta \longrightarrow \infty: \; f' = 0, \; g \longrightarrow 0, \; \theta \longrightarrow 0. \tag{14}$$

Here, prime denotes differentiation with respect to η, $K = \kappa/\mu$ is the material (micropolar) parameter, $\lambda = \frac{\gamma}{\mu j}$, is the microrotation density parameter, $\alpha = \alpha_1\left(\frac{U_0}{2\nu L}\right)^{\frac{1}{2}}$ is the velocity slip parameter, $\beta = \beta_1\left(\frac{U_0}{2\nu L}\right)^{\frac{1}{2}}$ is the thermal slip parameter, α_1 is the velocity slip factor, β_1 is the thermal slip factor (Mukhopadhyay (2013), $H_D = 2\left[\frac{\sigma_0 B_0^2 L}{\rho U_0} + \frac{\mu L}{\rho K_0}\right]$ is the Hartmann-Darcy number (the parameter accounting for the combined influence of the magnetic and the homogeneous porous medium permeability), $fw = -V_0\left(\frac{2L}{U_0\nu}\right)^{\frac{1}{2}}$ is the suction/injection parameter ($fw > 0$ suction , $fw < 0$ injection and $fw = 0$ corresponds to an impermeable sheet, $Pr = \frac{\mu C_p}{k}$ is the Prandtl number, $Q = 2Q_0\, \mathrm{L}/\rho U_0 C_p$ is the heat generation/absorption parameter, $Ec = \frac{U_0^2}{C_p T_0}$ is the Eckert number, $R = (4\sigma^* T_\infty^3)/\alpha^* k$ is the radiation parameter, $H = \frac{\nu L}{U_0 j_0}$ is the vortex viscosity parameter and $Gr = (2g\beta_0 T_0 L)/U_0^2$ is the Grashof number.

2. PHYSICAL QUANTITIES OF ENGINEERING INTEREST

The quantities of engineering interest are the non-dimensional skin friction, rate of heat transfer and the wall couple stress. These are respectively defined as [20]

$$C_{fx} = \frac{\tau_w}{\rho u_w^2}, \quad Nu_x = \frac{Lq_w}{k(T_w - T_\infty)}, \quad M_w = \left(\gamma \frac{\partial N}{\partial y}\right) \tag{15}$$

where

$$\tau_w = [(\mu + \kappa) + \kappa N]_{y=0}, \quad q_w = -k\left[\frac{\partial T}{\partial \bar{y}}\right]_{y=0} \tag{16}$$

are the wall shear stress and are the heat flux respectively.

In dimensionless form the skin friction, Nusselt number and wall couple stress correspondingly become

$$\frac{1}{\sqrt{2}}(Re_x)^{\frac{1}{2}} C_{fx} = \left(1 + (1 - nK)\right) f''(0), \quad \sqrt{2}(Re_x)^{-\frac{1}{2}} Nu_x = -\theta'(0), \tag{17}$$

$$M_w = \gamma \frac{u_w^2}{2\nu L} g'(0)$$

where $Re_x = \frac{u_w L}{\nu}$ is the local Reynolds number.

3. NUMERICAL SOLUTION

The coupled nonlinear differential equations (11-13) together with the boundary conditions (14) constitutes a two point boundary value problem (BVP) which are solved using shooting iteration technique alongside fourth order Runge-Kutta method. In this method, we have chosen a suitable finite value of $\eta \longrightarrow \infty$, say η_∞. The higher order nonlinear equations (11-13) which are of third order in f, and second order in both g and θ are reduced into a system of seven simultaneous equations of first order for seven unknowns. To solve this system, one needs seven initial conditions while only four initial conditions are available. Thus, there are still three initial conditions that are needed which are not given in the problem, these are: $f''(0), g'(0)$ and $\theta'(0)$. However, the values of f', g and θ are known as $(\eta_U, \eta_N, \eta_T) \longrightarrow \infty$. These three end conditions are used to produce the three unknown initial conditions (p_1, p_2, p_3) at $\eta = 0$ by applying the shooting technique.

To estimate the value of we start with some initial guess value and solve the BVPs equations (11-14) to get $f''(0), g'(0)$ and $\theta'(0)$. The procedure is repeated until two successive values of $f''(0), g'(0)$ and $\theta'(0)$ differ only after desired significant digit signifying the limit of the boundary along η. The last value of (η_U, η_N, η_T) are chosen as appropriate for a particular set of governing parameters for the determination of the dimensionless velocity $f'(\eta)$, microrotation $g(\eta)$ and temperature $\theta(\eta)$ across the boundary layer.

The higher order equations are reduced to a system of first order differential equations by letting:

$$f_1 = f, f_2 = f', f_3 = f'', f_4 = g, f_5 = g', f_6 = \theta, f_7 = \theta' \tag{18}$$

,

$$f_3' = \frac{2f_2'^2 - f_1 f_3 - K f_5 - Gr f_6 + H_D f_2}{(1+K)} \tag{19}$$

$$f_5' = \frac{3f_2 f_4 + 2KH(2f_4 + f_3) - f_1 f_5}{\lambda} \tag{20}$$

$$f_7' = \frac{-Pr(f_1 f_7 - 4f_6 f_2 + Q f_6 + Ec f_3^2 + Ec H_D f_2^2)}{\left(1 + \frac{4}{3}R\right)} \tag{21}$$

The boundary conditions now become

$$f_1(0) = fw, f_2(0) = 1 + \alpha f_3, f_3(0) = p_1, f_4(0) = -n f_3(0), f_5(0) = p_2$$
$$f_6(0) = 1 + \beta f_7, f_7(0) = p_3, \quad f_2(\infty) \longrightarrow 0, f_4(\infty) \longrightarrow 0, \quad f_6(\infty) \longrightarrow 0 \tag{22}$$

After obtaining all the initial conditions, fourth-order Runge-Kutta integration scheme with step size $\nabla\eta = 0.05$ is applied and the solution is obtained with a tolerance limit of 10^{-7}. The skin friction cofficient, the local Nusselt number and the wall couple stress are found from the numerical computations.

5. RESULTS AND DISCUSSION

In order to discuss the results effectively, the numerical computations are presented in the form of dimensionless velocity, temperature and microrotation profiles. The values of the controlling parameters namely: material (micropolar) parameter K, velocity slip parameter α, thermal slip parameter β, microrotation density parameter λ, vortex viscosity parameter H, Hartmann-Darcy parameter H_D, Prandtl number Pr, radiation parameter R, suction/injection parameter fw, Eckert number Ec *and* heat source (or sink) parameter Q.

Following the works of previous authors, we have chosen suitable values of the controlling parameters to determine their influence on the flow characteristics. The default values adopted for computation in this study are:

$$K = Gr = \lambda = H_D, \beta = 1.0, \alpha = 0.3, \ R = Ec = 0.1, fw = 0.5, Q = 0.2, n = 0.5, \ Pr = 0.71.$$

The graphs correspond to these values unless otherwise indicated on the graph.

In the absence of of the microrotation equation (Eq. 2), the material (micropolar) parameter K, the velocity and thermal slips parameters, the problem in this work reduces to that of Adeniyan and Adigun (2016). For the sake of validation with existing results of Bidin & Nazar (2009) and Mukhopadhyay (2013) we have replaced the coefficient "4" in the term $\theta f'$ in Eq. (13) by "1" as this does not affect the authencity of the present result. The numerical scheme is thus verified by making comparisons of the present results corresponding to the values of the Nusselt number $(-\theta'(0))$ with the existing work of Bidin & Nazar (2009), Mukhopadhyay (2013), Adeniyan & Adigun (2016) for some limiting situations. The comparisons are found to be in good agreement as shown in Table 1. Similarly, comparison of the values of the skin friction coefficient and the local Nusselt number obtained in this work agrees well with that of Seini and Makinde (2013) for some limiting situations as depicted in Table 2.

Table 1: Comparison of local Nusselt number $-\theta(0)$ for various values of Pr and R when $H_D, \alpha, \beta, Ec, H, Q, fw$ and R are all zeros

Pr	R	Bidin & Nazar (2009)	Mukhopadhyay (2013)	Adeniyan & Adigun (2016)	Present Results
1.0	0	0.9547	0.9547	0.95485201	0.9548106
3.0		1.8691	1.8691	1.869061724	1.8690688
5.0		-	2.5001	2.500122587	2.5001280
10.0		-	3.6603	3.660365072	3.6603693
1.0	1.0	0.5315	0.5311	0.537337859	0.5353012
2.0		1.0735	1.0734	-	1.0735162
3.0	0.5	1.3807	1.3807	-	1.3807451

Table 2: Comparison of the skin friction coefficient $f''(0)$ and Nusselt number $-\theta'(0)$ with Seini and Makinde for various values of R and Ec when $Pr = 0.71$, and $H_D, Ec, \alpha, \beta, fw, Q, R$ are zeros

		Seini & Makinde (2013)		Present Results	
R	Ec	$-f''(0)$	$-\theta'(0)$	$-f''(0)$	$-\theta'(0)$
0.0	1.0	1.629178	-0.006337	1.6291778	-0.0063379
0.1	1.0	1.629178	0.006964	1.6291778	0.0069647
0.5	1.0	1.629178	0.035754	1.6291778	0.0357547
0.1	2.0	1.629178	-0.598521	1.6291778	-0.5985207
0.1	3.0	1.629178	-1.204006	1.6291778	-1.2040062

Table 3 is a display of the values of skin-friction coefficient $f''(0)$ and rate of heat transfer $-\theta(0)$ of micropolar fluid as compared with the values for a Newtonian fluid for various values of the Hartmann-

Darcy parameter H_D, velocity slip parameter α, thermal slip parameter β and Eckert number Ec. From this table, it is observed that the values of the skin friction coefficient for a Newtonian fluid are higher than the corresponding values of the micropolar fluid with an increase in H_D, α, β and Ec. This table clearly shows that the micropolar fluid exhibits a reduction in the friction drag as compared to Newtonian fluid.
To be more specific, as the velocity slip parameter α rises from 0.1 to 3, the rate of increase in the skin friction coefficient is 78% in the micropolar fluid whereas the corresponding increase is 83% for the Newtonian fluid. Also, for H_D, the rate of increase in the skin friction coefficient is lower (68%) for the Newtonian fluid as compared to the micropolar fluid (80%) while the rate of heat transfer reduces by 23% for the Newtonian fluid with corresponding reduction of 19% for the micropolar fluid as H_D rises from 0 to 5.0.

Moreover, observation shows that the values of the Nusselt number indicating the heat transfer rate for the Newtonian fluid are lower than the corresponding values of the micropolar fluid with an increase in H_D, α, β and Ec. Specifically, the rate of heat transfer in the micropolar fluid reduces by 78% (or 14%) when β (or α) increases from 0.1 to 3 whereas this reduction is 77% (or 13%) in the Newtonian fluid. The rate of heat transfer also drops by 26% for the Newtonian fluid as Ec increases from 0.05 to 1.0 whereas this drop is only 10% in the micropolar fluid.

Table 3: Values $-f''(0)$ and $-\theta'(0)$ for variations in H_D, α, β and Ec.

				Micropolar Fluid		Newtonian Fluid	
H_D	α	β	Ec	$-f''(0)$	$-\theta'(0)$	$-f''(0)$	$-\theta'(0)$
0.0	0.3	1.0	0.1	0.5973747	0.5864942	0.8197306	0.5610731
1.0				0.7414607	0.5584511	0.9946504	0.5266762
3.0				0.9381281	0.5137339	1.2247594	0.4726876
5.0				1.0765975	0.4766906	1.3797858	0.4298266
1.0	0.1			0.9330780	0.5710755	1.3684405	0.5436416
	0.5			0.4395287	0.5281715	0.5177767	0.4951253
	1.5			0.3423427	0.5144845	0.3872402	0.4838322
	3.0			0.2068135	0.4907360	0.2210951	0.4672901
	0.3	0.1		0.6808540	1.1913225	0.8958823	1.0882682
		0.5		0.7414607	0.5584511	0.9946504	0.5266762
		1.5		0.7544545	0.4325054	1.0177197	0.4116810
		3.0		0.7730773	0.2584982	1.0528155	0.2499576
		1.0	0.05	0.7437231	0.5664145	0.9969028	0.5320998
			0.3	0.7325316	0.5269921	0.9857161	0.5051342
			0.6	0.7194555	0.4808902	0.9725144	0.4732391
			1.0	0.7025064	0.4212080	0.9552154	0.4313896

Table 4 illustrates the influences of the material parameter K, Prandtl number Pr, radiation parameter R, suction/injection parameter fw, Grashof number Gr and the microrotation density parameter λ on the

skin friction coefficient, the local Nusselt number (rate of heat transfer) and the wall couple stress coefficient. From this table, it is observed the skin friction coeffcient as well as the wall couple stress coefficient decreases with an increase in the material (micropolar) parameter K, radiation parameter R, injection parameter $fw < 0$, Grashof number Gr and the microrotation density parameter λ. On the other hand, the skin friction coefficient increases with Prandtl number and suction parameter respectively. Meanwhile, the parameters $K, Pr, fw > 0, Gr$ and λ enhance the local Nusselt number in the boundary layer while $R, fw < 0$ reduces the rate of heat transfer. This result indicates that the presence of micro-particles arising from the local structure and micromotion of the fluid particles tends to reduce the drag effect while enhancing the rate of heat transfer rate.

Table 4: Values $f''(0)$ $-\theta'(0)$ and $g'(0)$ for variations in K, Pr, R, fw, Gr and λ

K	Pr	R	fw	Gr	λ	$-f''(0)$	$-\theta'(0)$	$-g'(0)$
0.0	071	0.1	1.0	1.0	1.0	0.9946504	0.5266762	0.7687710
1.5						0.6677167	0.5668222	0.4659584
3.0						0.5247803	0.5811103	0.3100913
	1.0					0.7567499	0.6083422	0.5589718
	1.5					0.7711788	0.6636942	0.5693515
	2.5					0.7840882	0.7259503	0.5801830
		0.2				0.7359532	0.5418519	0.5460749
		0.4				0.7260094	0.5131326	0.5404235
		1.0				0.7028073	0.4503678	0.5279026
			-1.0			0.5590127	0.4883861	0.2820376
			-0.4			0.6240388	0.5149280	0.3648757
			0.4			0.7272081	0.5533926	0.5243001
			1.0			0.8167923	0.5843312	0.6955248
				0.0		0.8099592	0.5466010	0.6077389
				2.0		0.6806244	0.5667388	0.4932359
				5.0		0.5215765	0.5835472	0.3336177
					0.1	0.7361091	0.5595564	0.3992181
					2.0	0.7325289	0.5604010	0.3327680
					3.0	0.7276194	0.5616717	0.2652037

Figures 2-4 depicts the effects of the material parameter K on the dimensionless velocity, temperature and microrotation profiles respectively. It is noticed that the velocity as well as the momentum boundary layer thickness increases as the magnitude of K rises. The increase in the magnitude of K causes a reduction in the drag (see Table 4) which in turn enhances the motion of the fluid as shown in Figure 2. On the contrary, the temperature distribution across the boundary layer drops as K increases in magnitude as displayed in Figure 3. Also, the microrotation profiles decrease near the exponentially stretching sheet with an increase in K as illustrated in Figure 4.

The influence of the velocity slip parameter α on the velocity, temperature and microrotation profiles is shown in Figures 5-7. There is a reduction in the fluid motion as α increases as shown in Figure 5. It is

observed that the rate of transport reduces with the increasing distance (η) from the sheet for the velocity distribution. In the presence of slip, the stretching velocity and the flow velocity near the sheet are unequal. Hence, an increase in the slip parameter α causes a rise in the slip velocity which leads to a reduction in the fluid velocity. On the other hand, an increase in α enhances the temperature distribution due to the thickening of the thermal boundary layer thickness as shown in Figure 6. From Figure 7, it is noticed that the behaviour of the microrotation profiles is similar to that of the velocity profiles as α increases. Figure 8 reveals that an increase in the thermal slip parameter β causes a drop in temperature profiles as well as reducing the thermal boundary layer thickness. This response may be attributed to the fact that as β increases, less heat is transferred from the sheet to the fluid leading to a drop in the temperature. The effect of the microrotation density parameter λ on the microrotation profiles is exhibited in Figure 9. It is observed that the presence of the micro-particles enhances the microrotation profiles across the boundary layer.

Figures 10-12 show the combined influence of the magnetic and homogeneous porous medium permeability parameter known as Hartmann-Darcy parameter H_D on the velocity, temperature and microrotation profiles. It is observed that the fluid motion decreases as H_D rises as noted in Figure 10. This response is due to the imposition of the transverse magnetic field in an electrically conducting fluid which induces a retarding force known as Lorentz force acting against the fluid motion and slows it down. In addition, it is an indication that the permeability stabilizes the boundary layer growth. However, due to the resistance to the fluid motion imposed by both the Lorentz force and the Darcy force, the temperature rises with increasing values of H_D as displayed in Figure 11. These results clearly show that H_D can be used as a means of controlling the flow and heat transfer characteristics. An increase in the microrotation profiles is observed in Figure 12 close to the sheet whereas further from the sheet the opposite trend is observed as H_D rises in magnitude.

Figures 13-14 depict the influence of the suction/injection parameter fw on the velocity and temperature profiles. There is a reduction in the velocity and temperature profiles with an increase in the suction parameter ($fw > 0$). An increase in $fw > 0$ causes a thinning effect on both the velocity and temperature profiles due to the fact that the heated fluid is being pushed towards the sheet such that the fluid is brought closer to the surface which in turn leads to a reduction in the momentum and thermal boundary layer thicknesses. However, the imposition of wall fluid injection $fw < 0$ produces the opposite effect as it enhances velocity and thermal distribution across the boundary layer.

Figure 15 describes the influence of Eckert number Ec on the temperature profiles. Observation shows that increasing values of Ec enhances temperature distribution as well as the thermal boundary layer thickness. This response is due the fact that as Ec increases, heat is generated as a result of the drag between the fluid particles, the internal heat generation inside the fluid increases the bulk fluid temperature which is an indication of additional heating in the flow region due to viscous dissipation, thus, this additional heat causes increase in the fluid temperature. Figures 16-17 describe the influence of the Grashof number on the velocity and temperature.

It is clear from these figures that the velocity increases as the magnitude of Gr rises. From physical point of view, Gr represents the relative effect of the thermal buoyancy force to the viscous hydrodynamic force in the boundary layer. Thus, the motion of the fluid is accelerated by the enhancement in the buoyancy forces corresponding to an increase in Gr. The buoyancy forces behave as a favourable pressure gradient accelerating the fluid within the boundary layer. On the contrary, the temperature profiles reduce as the magnitude of Gr increases as shown in Figure 17.

The effect of radiation parameter R on temperature distribution is depicted in Figure 18. It is evident from this figure that thermal radiation enhances heat transfer since temperature profiles increase as R increases. Hence an increase in the magnitude of radiation parameter R, enhances the temperature in the boundary layer. This is due to the fact that the divergence of the radiative heat flux q_r increases as the Rosseland mean absorption coefficient α^* decreases (see Eq. 6). Figure 19 shows that the microrotation profiles increase with a rise in the magnitude of vortex viscosity parameter H.

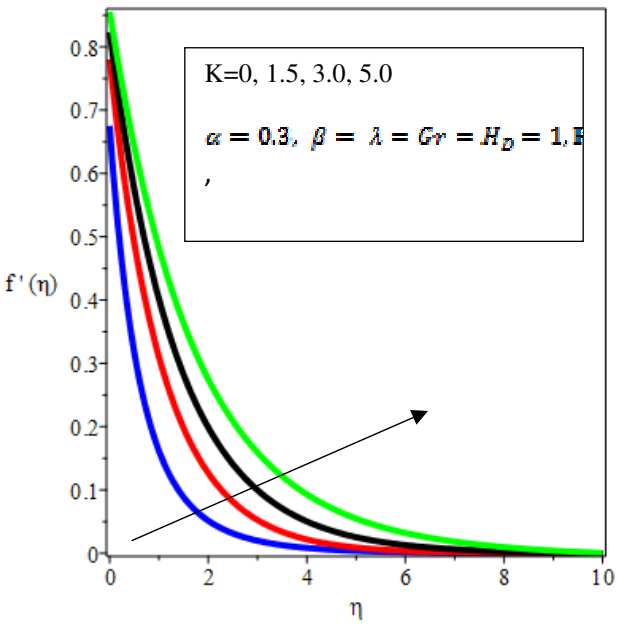

Figure 2. Effect of K on Velocity Profiles

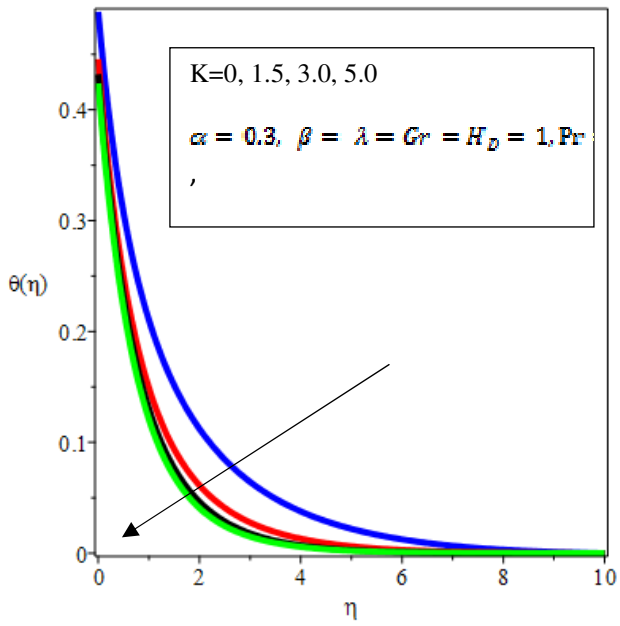

Figure 3. Effect of K on Temperature Profiles

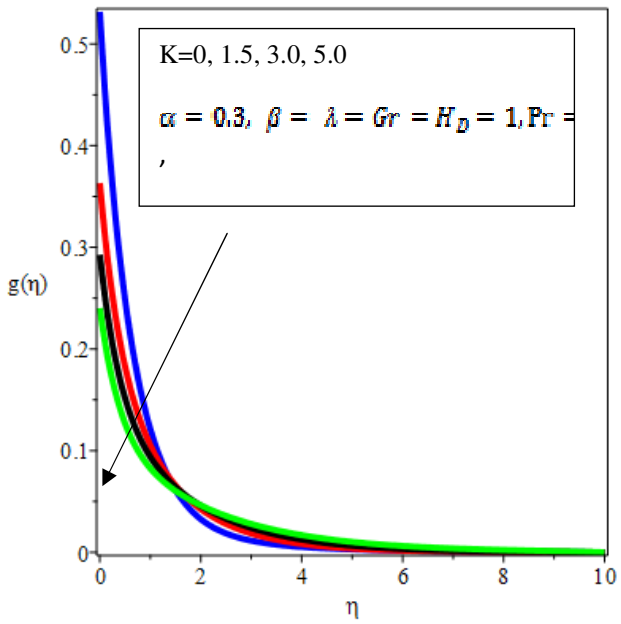

Figure 4 Effect of K on Microrotation

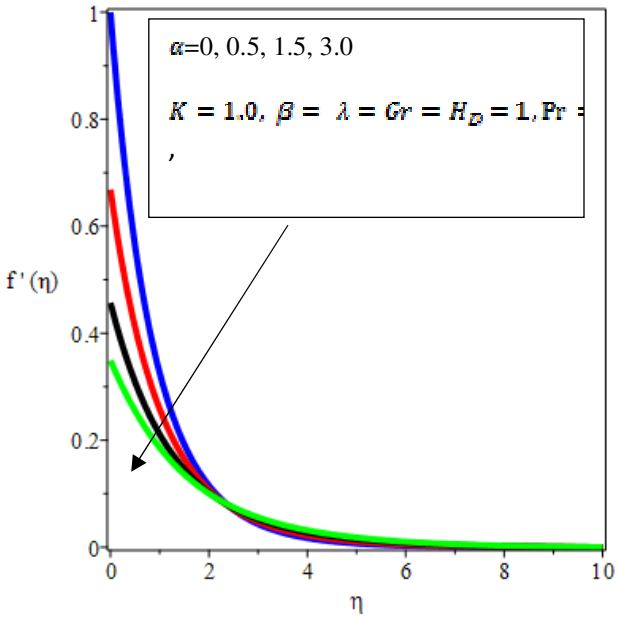

Figure 5. Effect of α on Velocity

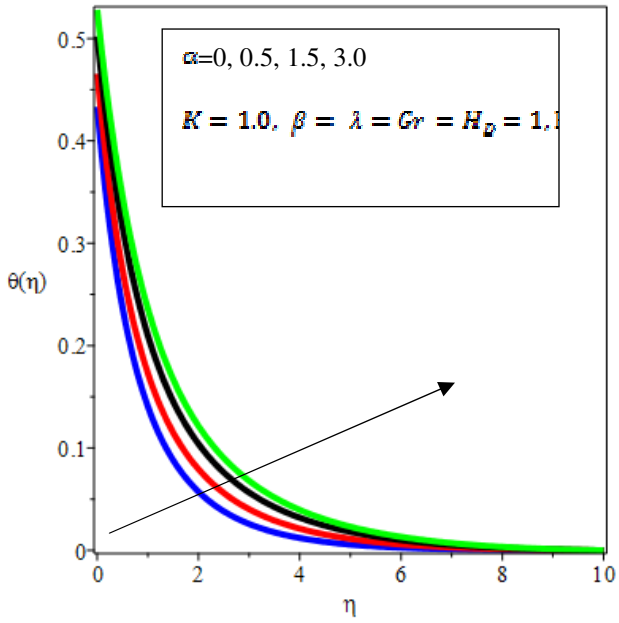

Figure 6. Effect of α on Temperature

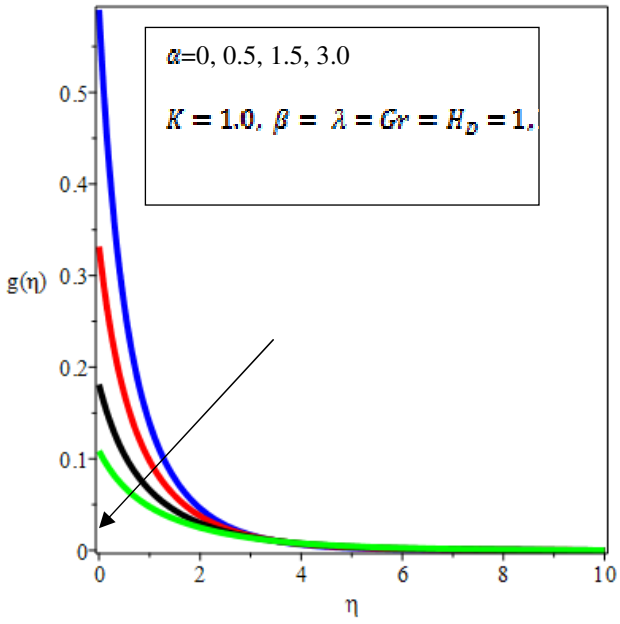

Figure 7. Effect of α on Microrotation

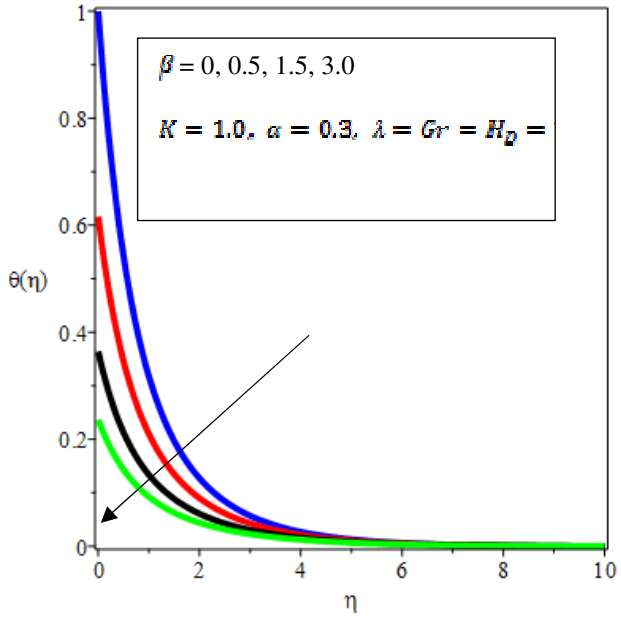

Figure 8. Effect of β on Temperature

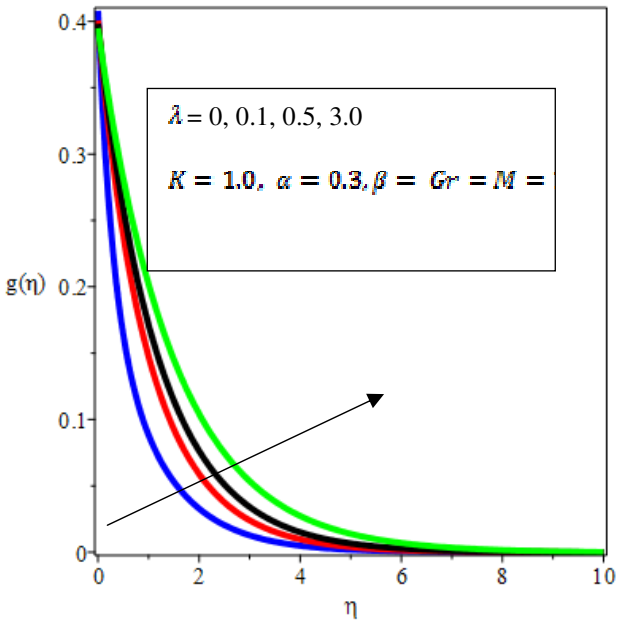

Figure 9. Effect of λ on Microrotation

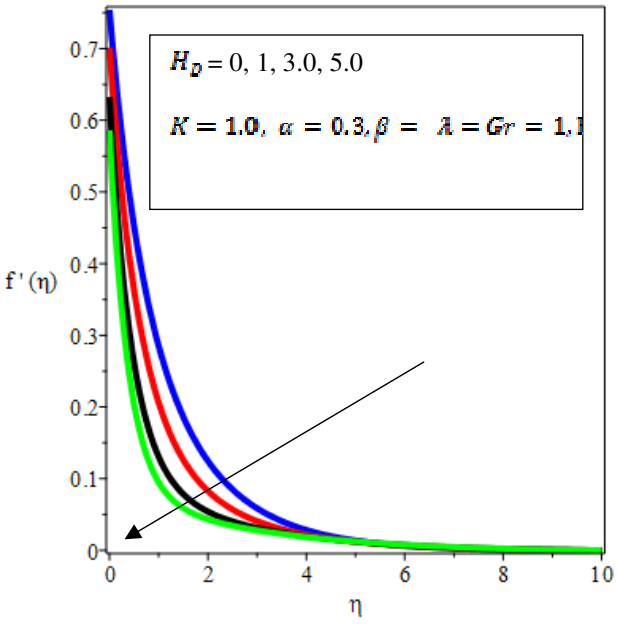

Figure 10. Effect of H_D on Velocity

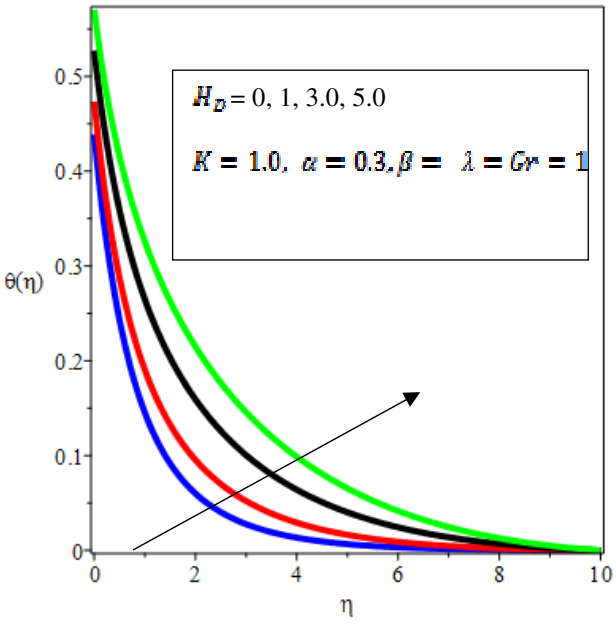

Figure 11. Effect of H_D on Temperature

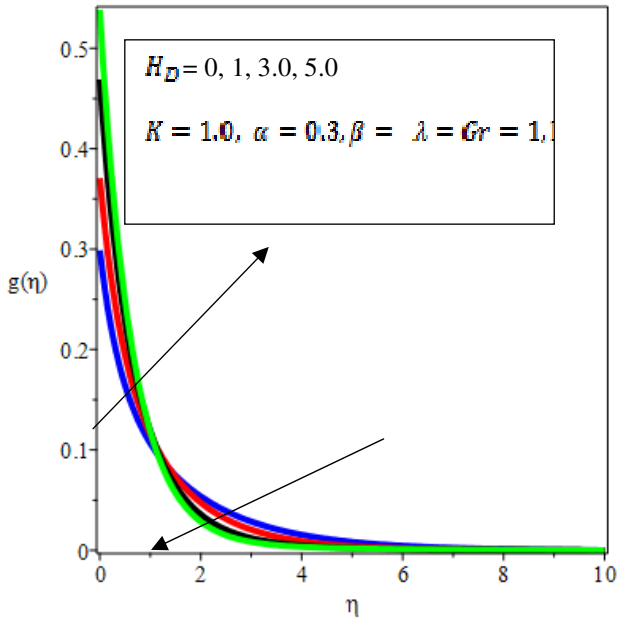

Figure 12. Effect of H_D on Microrotation

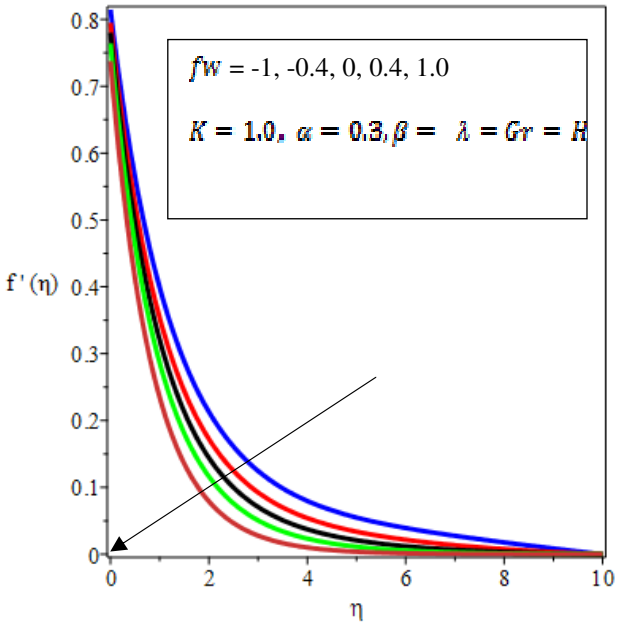

Figure 13. Effect of fw on Velocity

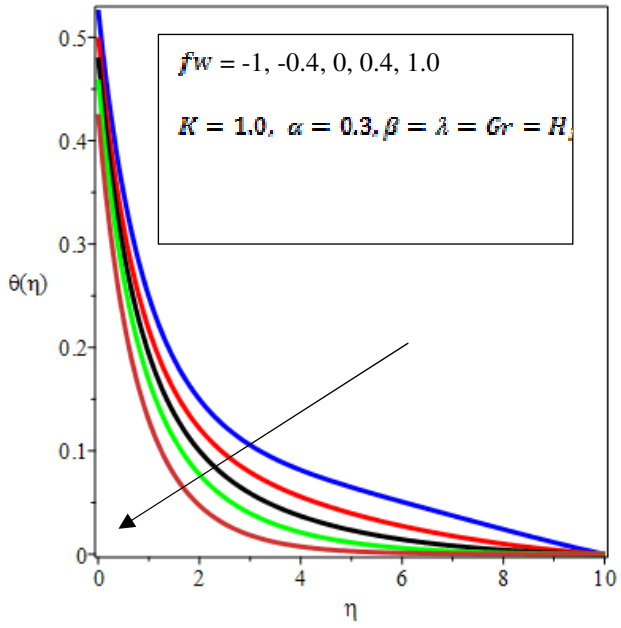

Figure 14. Effect of fw on Temperature

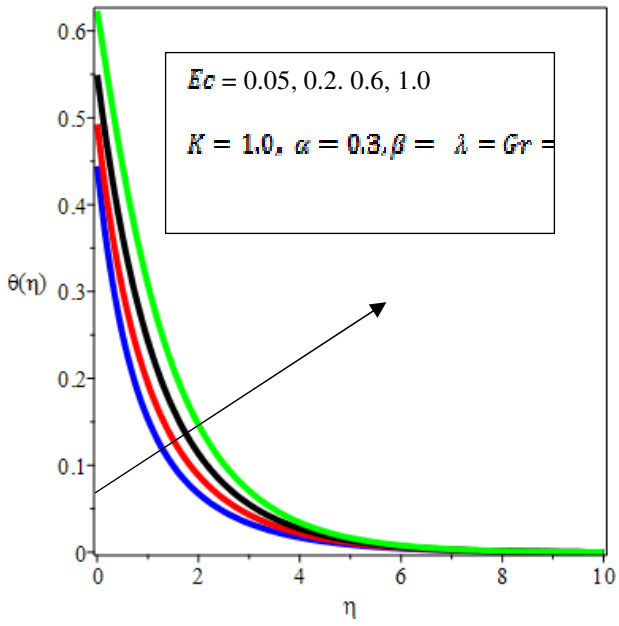

Figure 15. Effect of Ec on Temperature

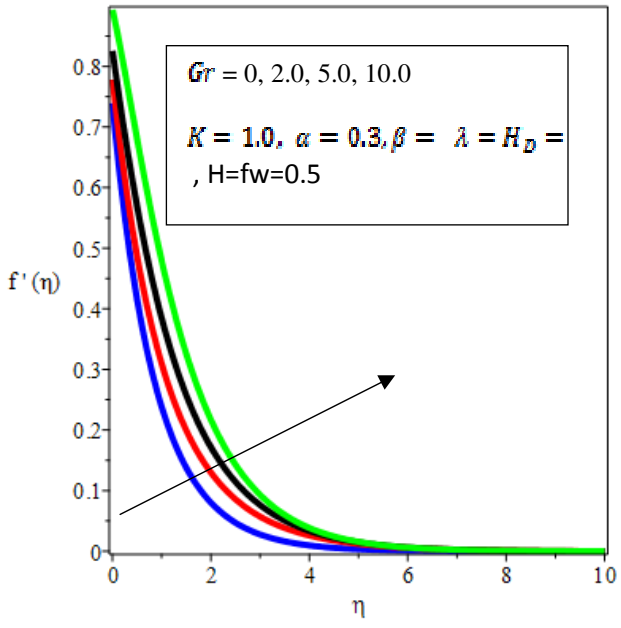

Figure 16. Effect of Gr on Velocity

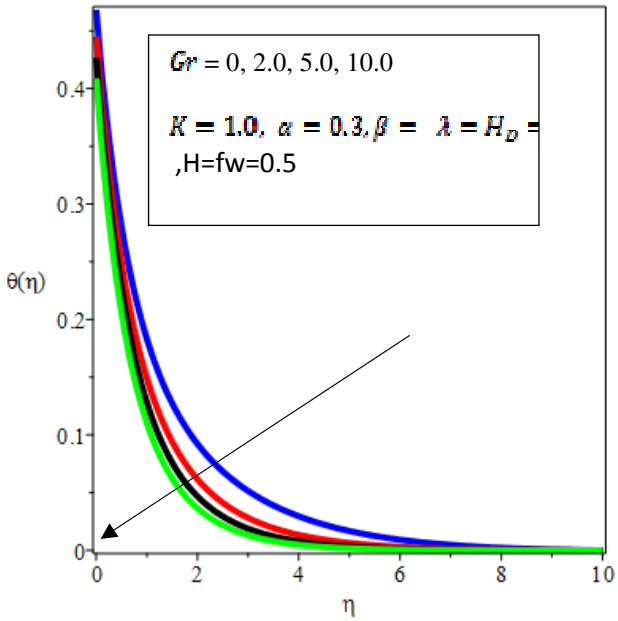

Figure 17. Effect of Gr on Temperature

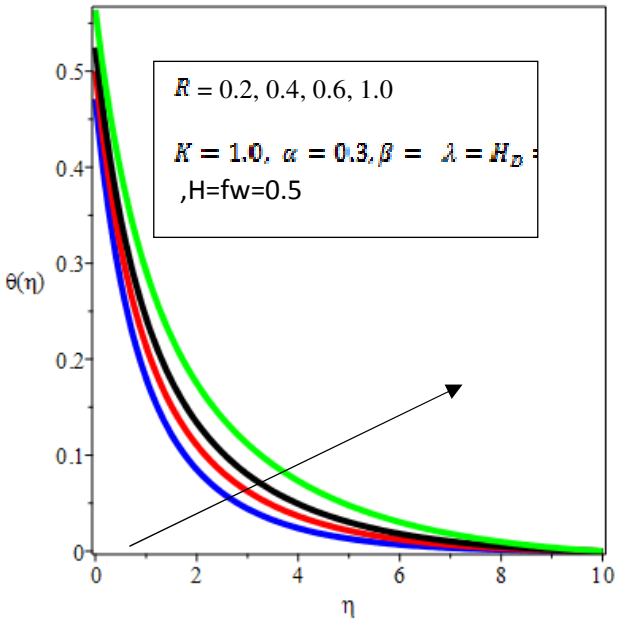

Figure 18. Effect of R on Temperature

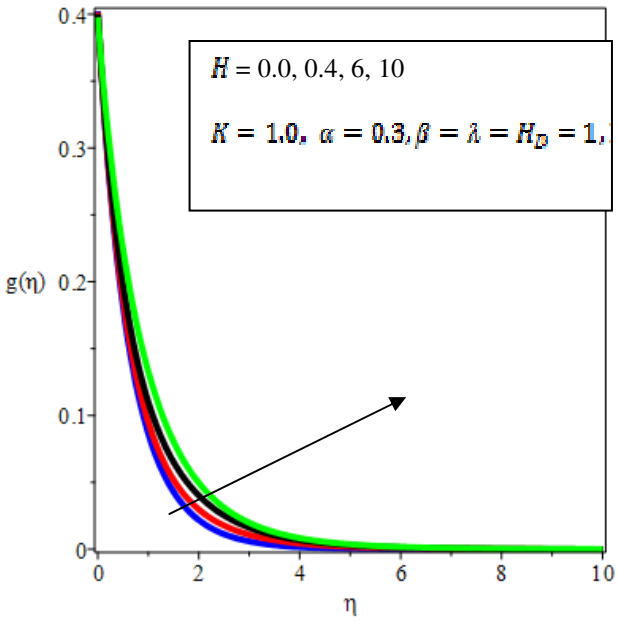

Figure 19. Effect of H on Microrotation

6. CONCLUSION

This study has investigated hydromagnetic flow and heat transfer of an incompressible electrically conducting micropolar fluid over an exponentially stretching vertical sheet abound in a saturated porous medium with slip effects. The influences of thermal radiation, viscous dissipation, heat source/sink, Joulean heating and suction/injection are also considered. The system of ordinary differential equations governing the fluid flow and heat transfer has been solved via shooting technique alongside fourth order Runge-Kutta integration scheme. The following conclusions are drawn from this study:

- The momentum as well as microrotation boundary layer thickness reduces with an increase in the velocity slip parameter α while the thermal boundary layer thickens with a rise in α but falls with an increase in the thermal slip parameter β.
- The values of the skin friction coefficient for a Newtonian fluid are higher than the corresponding values of the micropolar fluid for the parameters $H_D. \alpha, \beta, Ec.$
- The values of the Nusselt number indicating the rate of heat transfer for the Newtonian fluid are lower than the corresponding values of the micropolar fluid for the embedded controlling parameters.
- An increase in the magnitude of the velocity slip parameter causes a reduction in the skin friction while enhancing the rate of heat transfer. On the other hand, both the skin friction coefficient and the Nusselt number drops as the thermal slip increases.

REFERENCES

1. Adeniyan, A. (2015). MHD mixed convection of a viscous dissipating and chemically reacting stagnation-point flow near a vertical permeable plate in a porous medium with ther mal radiation and heat source/sink, *Asian Journal of Mathematics and Applications*, 1-23.
2. Adeniyan, A., and Adigun, J. A. (*2016*). Similarity solution of hydromagnetic flow and heat transfer past an exponentially stretching permeable vertical sheet with viscous dissipation, Joulean and viscous heating effects *Annals of Faculty Engineering Hunedoara- International Journal of Engineering,* 1-8.
3. Ahmadi, G. (1976). Self-similar solution of incompressible micropolar boundary layer flow over a semi-infinite plate, *Int. J. Engng Sci*, **14**, 639-646.
4. Akinbobola, T. E. and Okoya, S. S. (2015). The flow of second grade fluid over a stretching sheet with variable thermal conductivity and viscosity in the presence of heat source/sink, *Journal of Nigeria Mathematical Society*, **34**: 331-342.
5. Anderson, H. I. (2002). Slip flow past a stretching surface, Acta Mechanica, **158**: 121-125.
6. Bidin, B and Nazar, R. (2009). Numerical solution of the boundary layer over an exponentially stretching sheet, *European Journal of Scientific Research*, **33:** 710-717.
7. Bugliarello, G. and Hayden J. W. (1962). High speed microcinematographic studies of blood flow in vitro. *Science,* **138**: 981–983.
8. Chen, J., Liang, C. and Lee J. D. (2011). Theory and simulation of micropolar fluid dynamics, J. Nanoengineering and nanosystems, **224**: 31-39.
9. Crane, L. J. (1970). Flow past a stretching plate*, Communicatios Breves*, **21**: 645-647.
10. Das, K. (2012). Slip effects on heat and mass transfer in MHD micropolar fluid flow over an inclined plate with thermal radiation and chemical reaction*, Int. J. Numer. Meth. Fluids*, doi:10.2002/fd.2683.
11. Devi, R. L., Neeraja, A. and Reddy, N. B. (2015). Radiation effect on MHD slip flow past a stretching sheet with variable viscosity and heat source/sink, *Int. J. Sci and Innovative Mathematical Res,* **3**: 8-17.
12. El-Aziz, M. (2009). Viscous dissipation effect on mixed convection flow of a micropolar fluid over an exponentially stretching sheet, *Can. J. Phy*, **87**, 359-368.
13. Eldabe, N. T., Elshehawey, E. F., Elbarbary, M. E. and Elgazery, N. S. (2003). Chebyshev finite difference method for MHD flow of a micropolar fluid past a stretching sheet with heat transfer, Journal of Applied Mathematics and Computation, **160**: 437-450.
14. Eringen, A. C. (1966). Theory of micropolar fluids, J. Math. Anal. Appl., **16**: 1-18.
15. Eringen, A. C. (1972). Theory of thermo-microfluids, Journal of Mathematical Analysis and Applications, **38**: 480-496.
16. Fatunmbi, E. O and Fenuga, O. J. (2017). MHD micropolar fluid flow over a permeable stretching sheet in the presence of variable viscosity and thermal conductivity with Soret and Dufour effects, *International Journal of Mathematical Analysis and Optimization: Theory and Applications*, **2017**: 211- 232.

17. Fatunmbi, E. O. and Adeniyan, A. (2018). MHD stagnation point-flow of micropolar fluids past a permeable stretching plate in porous media with thermal radiation, chemical reaction and viscous dissipation, *Journal of Advances in Mathematics and Computer Science,* **26**: 1-19.
18. Gupta, P. S. and Gupta, A. S. (1977). Heat and mass transfer on a stretching sheet with suction or blowing, *Can. J. Chem. Eng*, **55**: 744-746.
19. Hayat, T., Shehzad, S. A. and Qasim, M. (2011). Mixed convection flow of a micropolar fluid with radiation and chemical reaction, *Int J. Numer Meth*, **67**:1418-1436.
20. Jena, S. K. and Mathur, M. N. Similarity solutions for laminar free convection flow of a thermomicropolar fluid past a non-isothermal flat plate, *Int. J. Eng. Sci.* **19**, 1431-1439.
21. Lukaszewicz, G. *Micropolar fluids: Theory and Applications*, 1st Ed., Birkhauser, Boston, 1999.
22. Magyari, E and Keller, B. (1999). Heat and mass transfer in the boundary layers on an exponentially stretching continuous surface *Journal of Physics*, **32**: 577-585.
23. Makinde. O. D. (2010). Similarity solution of hydromagnetic heat and mass transfer over a vertical plate
24. with a convective surface boundary condition. *Int. Journal of the Physical Sciences*. **5**: 700-710.
25. Mandal, I. and Mukhopadhyay, S. (2013). Heat transfer analysis for fluid flow over an exponentially stretching porous sheet with surface heat flux, *Ain Shams Eng. Journal*, 103-110.
26. Mukhopadhyay, S. (2013). Slip effects on MHD boundary layer flow over an exponentially stretching sheet with suction/blowing and thermal radiation, *Ain Shams Engineering Journal*, 485-491.
27. Nandeppanavar, M. M., Vajravelu, K., Abel, M. S and Siddalingappa, M. N. (2013). MHD flow and heat transfer over a stretching surface with variable thermal conductivity and partial slip, *Meccanica*, **48**: 1451-1464.
28. Nubar Y. (1971). Blood flow, slip and viscometry. *Biophysics Journal,* **11**:252–264.
29. Olajuwon, B.I., Oahimire, J. I. and Waheed, M.A. (2014). Convection heat and mass transfer in a hydromagnetic flow of a micropolar fluid over a porous medium, *Theoret. Appl. Mech.* 41: 93-117.
30. Peddieson, J and McNitt, R. P. (1970). Boundary layer theory for micropolar fluid, *Recent Adv. Enggng Sci.*, **5**, 405.
31. Peddieson, J. (1972). An application of the micropolar model to the calculation of a turbulent shear flow, *Int. J. Eng. Sci.*, **10:** 23-32.
32. Reddy, M. G. (2012). Heat generation and thermal radiation effects over a stretching sheet in a micropolar fluid, *International Scholarly Research Networks,* **2012**: 1-6 doi.org. /10.5402/2012/795814.
33. Seini, Y. I. and Makinde, O. D. (2013). MHD boundary layer flow due to exponentially stretching surface with radiation and chemical reaction, *Mathematical Problem in Engineering*, 1-7.
34. Srinivasacharya, D. and RamReddy, Ch. (2011). Soret and Dufour effects on mixed convection from an exponentially stretching surface. *Int. J. of Nonlinear Sci.* **12:** 60-68.
35. Wang, C. Y. (2002). Flow due to stretching boundary with partial slip- an exact solution of the Navier Stokes equation, *Chen Eng. Sci.,* **57**: 3745-3747.